Comparison of Generative AI Design Optimization on a Transonic Wing with CFD Analysis

Jason S. Rupram*
University of Georgia, Athens, Georgia, 30602, United States

Generative Artificial Intelligence (AI) is a rapidly evolving branch of AI that uses algorithms and data sets of existing research to predict the outcomes of new designs. The traditional gradient based aerodynamic optimization method utilizes adjoint solvers that explore large multidimensional design spaces to achieve optimal geometry for the required flight profile. This project focused on optimizing a transonic wing to improve the overall L/D ratio using the generative AI tools o1, o3, and DeepSeek R1 instead of industry accepted gradient based optimization. The ONERA M6 wing served as the baseline model, allowing for accurate simulation data comparison. This design was modeled using OpenVSP and simulated in ANSYS Fluent with the k omega SST and Spalart Allmaras turbulence models. Aerodynamic features such as shock wave formation, pressure distribution, and total L/D were analyzed and compared using the experimental data. The results from the optimized wing geometries demonstrated a decrease from the original L/D of 12.86 under the flight condition of Mach 0.84 and AoA of 3.06 degrees.

I. Nomenclature

AR	=	Aspect Ratio
AoA	=	Angle of Attack
c	=	Chord Length
C_D	=	Drag Coefficient
C_L	=	Lift Coefficient
L/D	=	Lift to Drag Ratio
C_M	=	Moment Coefficient
C_p	=	Pressure Coefficient
R_e	=	Reynolds Number
b	=	Wingspan
ρ	=	Fluid density
μ	=	Dynamic Viscosity
ν	=	Turbulent Viscosity

II. Introduction

Conventional gradient driven approaches used adjoint and sensitivity frameworks to utilize multidimensional design spaces and ensure optimal designs. Generative AI had the potential to accelerate this process by offering quick, data informed design seeds, helping engineers explore non intuitive design variable combinations before refining them through rigorous gradient based loops.

In this project, o1, o3, and DeepSeek R1 were employed to propose transonic wing modifications, specifically targeting improvements in the lift to drag ratio. As a baseline, the ONERA M6 wing was selected due to its extensive validation history and well documented aerodynamic characteristics. Following baseline validation, the models received simulation data such as C_L, C_D, L/D, boundary conditions, and fluid properties. They were then tasked with proposing optimized wing geometries that mitigated shock induced flow separation and reduced wave drag. A comparison study assessed whether any of the generated designs demonstrated superior performance compared to the baseline model.

*Graduate Student, School of Environmental, Civil, Agricultural, and Mechanical Engineering.
AIAA Control ID: 1785154

III. Relevant Literature Review

In the past decade, research in the field of generative design has seen a drastic increase in the areas of manufacturing, marketing, education, etc. There have been recent studies regarding the use of AI and Large Language Models (LLMs) in the field of manufacturing and even aerospace design, specifically one paper coming from The University of Georgia. Li et al. demonstrated the outstanding capabilities of LLMs in taking complex prompts and instructions and extracting knowledge from a large amount of data to solve problems [1]. A thorough investigation conducted by Makatura et al. at MIT assessed GPT's performance in five vital CAx areas: design creation, exploration of design spaces, design for manufacturing (DfM), performance assessment, and inverse design [2]. In addition, research has been published on the use of machine learning models for aerodynamic analysis [3–5].

IV. Preliminary and Final Design Concept

In the preliminary design stage, the core objectives and initial geometries were identified, establishing the foundation for all subsequent analyses. Based on iterative feedback and basic aerodynamic considerations, various refinements were then explored to address performance, feasibility, and cost constraints. Ultimately, the final design concept integrated these refinements into a cohesive solution, ensuring that key requirements were met and validated under representative conditions.

A. Preliminary Design Concept

Initial research focused on what the baseline model should be so that the generative models could be trained to identify key data points and optimize them for higher efficiency. NASA resources contained a CFD simulation setup for the ONERA M6 wing and validation from wind tunnel testing. This wing used a symmetric airfoil with an inlet speed of Mach 0.84 and an AoA of 3.06°. With this experimental data widely available, the CFD simulation could determine pressure coefficients, shock wave formation, flow separation, lift, and drag to compare the results.

B. Final Design Concept

The final design concept was featured around the ONERA M6 wing, first tested in 1979 (Schmitt & Charpin), but later used by NASA's Langley Research Center (LRC) to conduct a numerical analysis of turbulence model simulations [6, 7]. This baseline model was chosen because of the detailed simulation and experimental data provided by NASA such as geometric properties, initial conditions, modeling equations, turbulence model, lift coefficients, and drag coefficients. Additionally, for specific transonic flight simulations, the ONERA M6 wing was widely used amongst the aerospace community to set baseline models for CFD analysis in aerodynamic research and served as a reference to validate CFD methods [8–14]. ANSYS also used the ONERA wing as a training model in beginning aerodynamic CFD simulations for CFD training purposes.

V. Design Parameters of Baseline Model

OpenVSP was utilized to create the baseline CAD model as well as the optimized design models produced from the generative models. OpenVSP created the CAD model due to its benefits of being able to quickly modify the wing based on different design parameters, unlike traditional CAD software, which required the user to start from the beginning for each model.

Table 2 ONERA M6 Wing Geometry

Geometric Properties	
Span	1.1963 m
Mean Aerodynamic Chord	0.64607 m
Root Chord	0.80590 m
Aspect Ratio	3.8
Taper Ratio	0.562
Leading Edge Sweep	30°
Trailing Edge Sweep	15.8°

This section detailed the initial design parameters and data for the ONERA M6 wing. The airfoil used for this wing featured a symmetrical airfoil, for which the DAT file could be found on the NASA LRC turbulence modeling resource page[8]. Using the relationship between the root chord of the wing and the taper ratio, the value for the tip chord was found to be 0.45292 m. It should be noted that the original wing featured a rounded tip semi span of 1.2185 m. This was not available to model exactly in OpenVSP, however, to accomplish this design, the rounded tip cap feature was selected within OpenVSP. Figures 1a and 1b displayed the baseline CAD model of the ONERA M6 wing. Since OpenVSP could only produce a collection of surface models rather than closed bodies, the wing was imported to Fusion360, where the surfaces were stitched to form one single body.

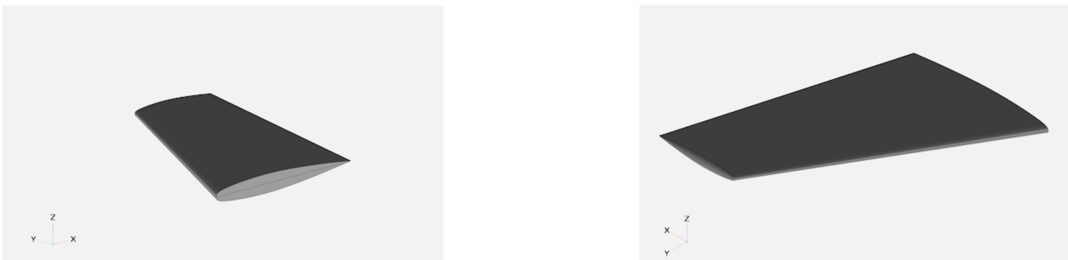

(a) Left View **(b) Right View**

Fig. 1 OpenVSP ONERA M6 Wing Model

VI. Modeling Assumptions

For this project, several modeling assumptions could be made about the air flowing over the wing in the transonic regime.

1. Airflow was compressible ($\rho \neq$ constant)
2. Non constant fluid properties
3. Steady state (d/dt = 0)
4. Turbulent flow
5. 3D flow
6. Viscous flow near and around wing model

VII. Modeling Equations

From the Schmitt and Charpin paper, the airflow had a Reynolds number (1) of 11.72E+06. This value could be used to calculate the density of air entering the system from the Reynolds number equation for flow over a flat plate.

$$R_{e_L} = \frac{\rho V L}{\mu} \tag{1}$$

As a result of the compressible airflow assumption, the ideal gas law (2) was used to account for the changing density of the air.

$$P = \rho R T \tag{2}$$

The dynamic viscosity of air for this simulation was calculated using Sutherland's Law.[7]

$$\mu = \mu_{ref} \left(\frac{T}{T_{ref}} \right)^{3/2} \left(\frac{T_{ref} + S}{T + S} \right) \tag{3}$$

Lastly, the turbulent viscosity of air was calculated using the following equation:

$$\nu_{\text{farfield}} = 3 \frac{\mu}{\rho} \tag{4}$$

VIII. Boundary and Initial Conditions

To accurately compare the baseline simulation to the experimental data, the model contained a pressure far field around the wing in which the air ambient pressure could be calculated from Eq. 2 to 98,858.97 Pa, and the temperature was 300 K. The wing acted as a wall with a no slip boundary condition, meaning the velocity of the air was zero at the surface. The freestream airflow around the wing was Mach 0.84 with an AoA of 3.06° and a Reynolds number of 11.72E+06.

IX. ONERA M6 Simulation

A. Geometric Setup and Meshing

After creating and meshing the wing geometry, the final mesh consisted of 4,358,399 elements and 1,622,520 nodes, characterized by an average skewness of 0.20983 and a minimal orthogonal quality of 0.7876.

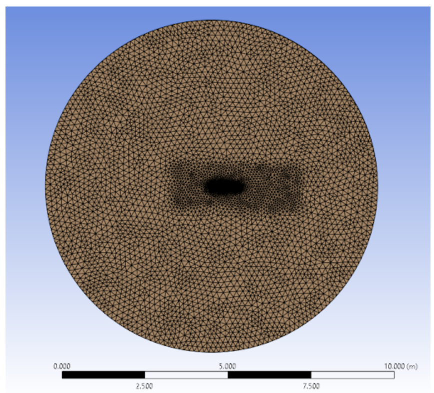

Fig. 2 Conducted Mesh with nodes and elements in ANSYS Mechanical.

B. Results

The baseline model provided CFD analysis of the L/D, shock wave formation, and the static pressure distribution across the entire wing. First, it was important to analyze the static pressure over the entire wing, as this set the basis of what to expect from the lift and drag coefficients as well as the shock wave across the wing. From this, a high stagnation pressure zone formed at the leading edge of the wing of 150,000 Pa. On top of the airfoil, the pressure significantly dropped to around 67,000 Pa and formed an almost conical shape, demonstrating lift generation. The static pressure instantaneously increased after this region and stayed constant until reaching the trailing edge, where it was assumed that flow separation had occurred causing the airflow to decrease.

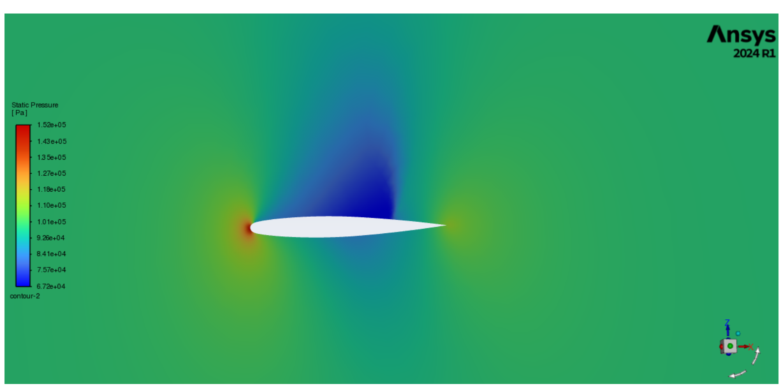

Fig. 3 Static Pressure Distribution Airfoil.

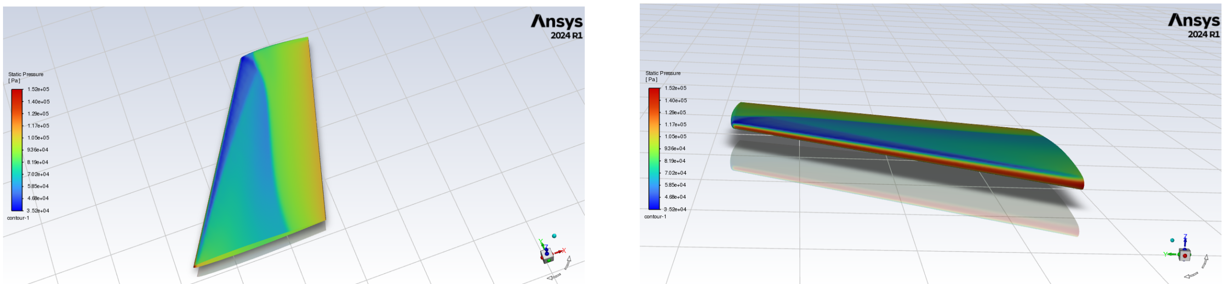

(a) Top View **(b) Right View**

Fig. 4 Wing Static Pressure Distribution

Fig. 4 shows the pressure distribution across the wing. The pressure variation provided an image of the shock wave formed across the top surface of the wing. The shock wave formed closer to the trailing edge at the root of the wing and moved closer to the trailing edge at the tip. The delayed onset of the shock formation at the root wing was a result of the sweep geometry of the ONERA M6 wing.

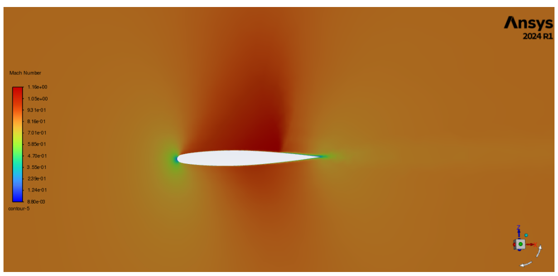

Fig. 5 Mach Number Distribution.

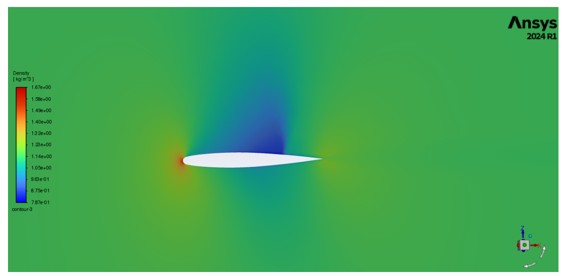

Fig. 6 Density Distribution.

It was also beneficial to analyze the Mach number contour and the density contour of the air as it flowed over the surface of the airfoil. It should be noted that the flow was locally supersonic over the top of the wing, ultimately causing the shock wave formation. At an initial Mach number of 0.84, the symmetrical ONERA M6 airfoil caused the flow to accelerate to a value of Mach 1.16. The density contour demonstrated the low density region before the shock wave formation, decreasing to roughly 0.787 kg/m^3, and then the instantaneous increase in air density directly after the shock wave to a value of 1.23 kg/m^3.

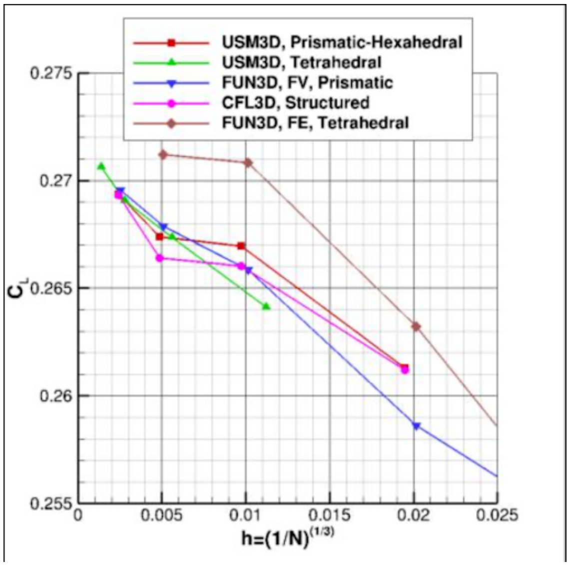

Fig. 7 ANSYS Simulation

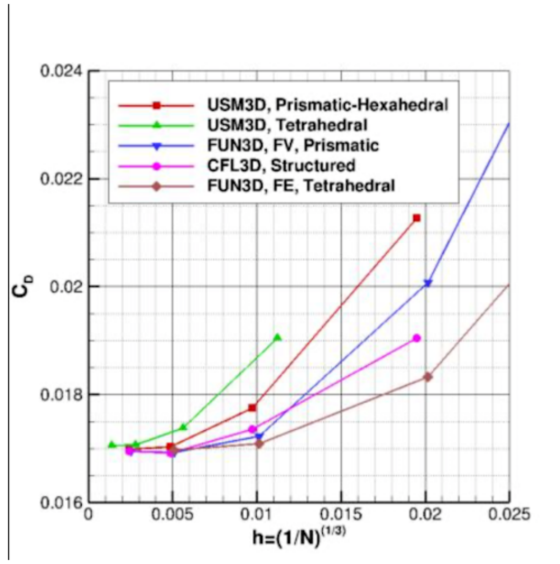

Fig. 8 Experimental Data

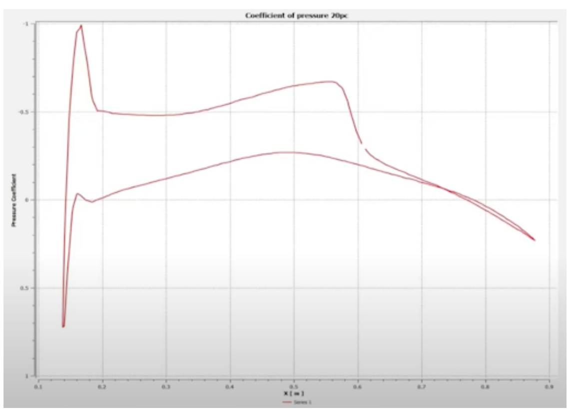

Fig. 9 ANSYS Simulation

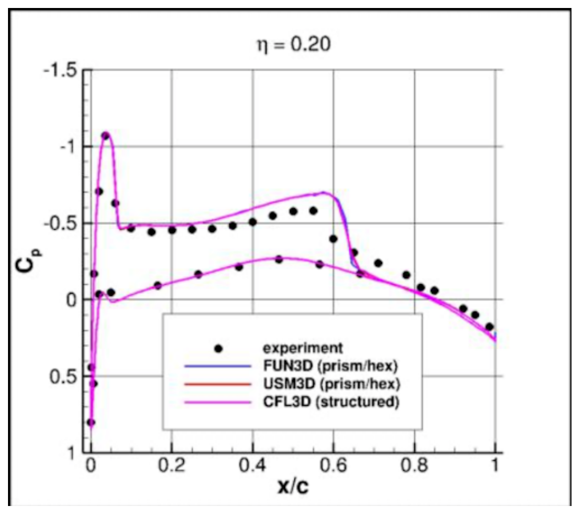

Fig. 10 Experimental Data

It was important to compare the pressure coefficients across the airfoil at various locations along the wing to the experimental results from NASA. However, to save computational time, it was reasonably assumed that comparing only one plot was sufficient enough in concluding the accuracy of the simulation in this report. The plots were compared at 20 percent of the span from the root of the wing.

This section provided insight into the simulation setup and results, analyzing the L/D of the wing at Mach 0.84 and an AoA of 3.06, as well as the shock wave formation along the span of the wing and the static pressure distribution.

X. Design Parameters of Optimized Models

The following prompt was outlined for the generative models:

> I am running an ANSYS CFD simulation on the ONERA M6 wing, in which all geometric properties of the wing can be found online. This simulation is run with inlet conditions of Mach 0.84, a pressure far field of 98858.97 Pa, a boundary condition temperature of 300 K, a Reynolds number of 11.72E+06, a turbulent

viscosity of $1.8459E - 05\ N * s/m^2$, and an AoA of 3.06. The initial density can be calculated using the ideal gas law, and the dynamic viscosity can be calculated from Sutherland's Law. Attached are the lift and drag coefficients, shock wave formation, static pressure over the airfoil, and pressure coefficients at 20 percent of the span resulting from the CFD simulation using the Spalart Allmaras turbulence model. After analyzing the initial conditions provided, as well as the wing model and the results from the CFD simulation, can you specifically name your top two recommendations for optimizing this model to increase lift, minimize the impact of shock waves on shock induced separation and wave drag, and ultimately optimize the pressure distribution over the entire wing and airfoil. Be specific in your answers, meaning provide specific values that you would recommend, such as different airfoils, changes to the geometry, etc., and do not recommend changes to the mesh quality for the sake of fair and accurate comparisons between models. Thank you.

A. AI Model Discussion and Geometry

Table 3 o1 Geometry

Geometric Properties	
Airfoil	NASA SC(2)-0714
Span	1.1963 m
Mean Aerodynamic Chord	0.62940 m
Root Chord	0.80590 m
Aspect Ratio	3.8
Taper Ratio	0.562
Leading Edge Sweep	30°
Trailing Edge Sweep	15.8°
Twist	2° Half Span

Table 4 o3 Geometry

Geometric Properties	
Airfoil	NASA SC(2)-0714
Span	1.1963 m
Mean Aerodynamic Chord	0.62940 m
Root Chord	0.80590 m
Aspect Ratio	3.8
Taper Ratio	0.562
Leading Edge Sweep	30°
Trailing Edge Sweep	15.8°
Twist	2° Full Span

XI. AI Models Optimzed ANSYS Simulation

A. o1 Simulation Results

The static pressure over the NASA SC(2)-0714 wing displayed shock wave formation from the wing root to the tip that appeared to oscillate when compared to the baseline ONERA M6 wing. The static pressure initially rose to about 156,000 Pa at the leading edge, then dropped to around 60,000 Pa across the upper surface of the wing. Immediately past the shock wave, the static pressure returned to roughly 100,000 Pa. This pressure jump helped produce a higher lift coefficient.

In the density contour, the air density decreased to about 0.8 kg/m^3 before the shock wave and then increased to roughly 1.1 kg/m^3 immediately afterward. In the Mach number contour, the freestream Mach 0.84 flow accelerated to approximately Mach 1.4 at the shock. Because the AoA was steeper than the ideal for the airfoil, the flow struggled to stay attached in the aft region of the airfoil, producing more drag.

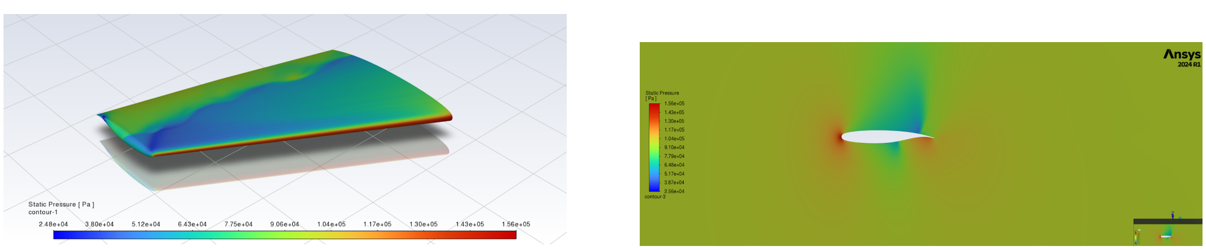

(a) Wing **(b) Airfoil**

Fig. 11 o1 Static Pressure Distribution

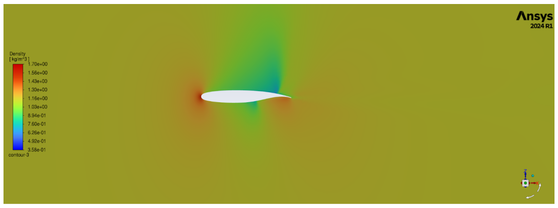

Fig. 12 o1 Density Distribution.

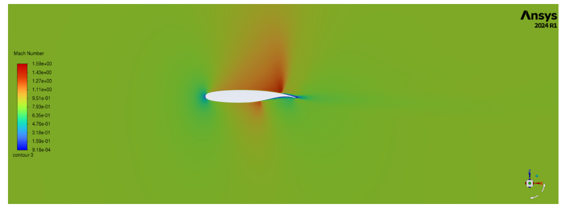

Fig. 13 o1 Mach Number Distribution.

The C_L and C_D values produced from the o1 optimized wing model displayed oscillations consistent with shock buffeting. The C_L curve fluctuated between 0.51 and 0.53, with an average C_L of 0.52, and the C_D curve fluctuated between 0.06 and 0.059, averaging approximately 0.0595. This increase in drag offset the gains in lift, leading to a lower L/D of 8.79 compared to the baseline.

B. o3 Simulation Results

The o3 optimized wing utilized the NASA SC(2)-0714 airfoil with a full span washout twist. In the density contour, the air density decreased to about 0.75 kg/m^3 before the shock wave and then increased to roughly 1.1 kg/m^3 immediately afterward. In the Mach number contour, the freestream Mach 0.84 flow accelerated to approximately Mach 1.45 at the shock. Due to the AoA being steeper than the ideal for the airfoil, the flow struggled to stay attached in the aft region of the airfoil.

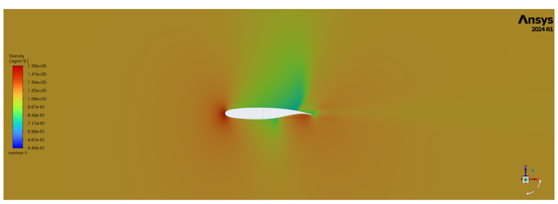

Fig. 14 o3 Density Distribution.

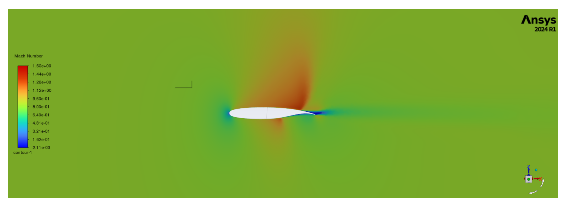

Fig. 15 o3 Mach Number Distribution.

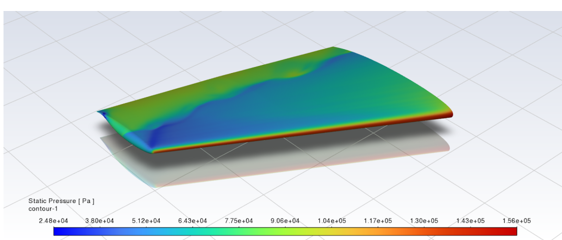

(a) Wing

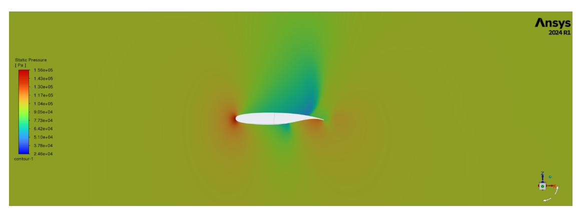

(b) Airfoil

Fig. 16 o3 Static Pressure Distribution

From the Mach number contour and density contour, it was evident that a localized region on the underside of the wing briefly exceeded Mach 1, indicating the presence of a weak shockwave. This shock was significantly weaker than the one on the upper surface. On the upper surface, the air accelerated more aggressively due to higher camber, leading to a stronger and more abrupt transition from supersonic to subsonic flow. The lower surface experienced a smaller section of supersonic flow, with a gradual shift back to subsonic speeds. This smoother transition was reflected in the Mach number contours, where there was no sharp color boundary to indicate a severe shock.

The o3 model displayed oscillations for both coefficients caused by shock buffeting, with C_L varying from 0.56 to 0.59, averaging approximately 0.575. The C_D ranged between 0.068 and 0.066, with an average of roughly 0.067. Although it achieved higher lift than the o1 model, it also produced higher C_D, resulting in an L/D of 8.58.

XII. Comparison of Results

To accurately compare the simulation results, the percentage difference in L/D for each model was compared to the baseline model:

$$\text{Score} = \left(\frac{(L/D)_{\text{New}} - (L/D)_{\text{Base}}}{(L/D)_{\text{Base}}} \right) \times 100 \tag{5}$$

Table 5 Model Comparison Data

Model	L/D	Score
Baseline	12.86	N/A
o1	8.79	- 32.27%
o3	8.58	- 33.28%

The results of the CFD simulations showed that the optimized wings did not surpass the ONERA aerodynamic efficiency under the flight conditions of Mach 0.84 and AoA of 3.06. The data indicated that the recommended geometric changes increased peak lift while increasing drag, primarily due to shock induced separation and unsteady behavior consistent with shock buffeting.

XIII. Conclusions

The main goal of this report was to analyze whether the designs provided by o1, o3, and R1 enhanced aerodynamic characteristics of the ONERA M6 wing under the flight condition of Mach 0.84 and an AoA of 3.06°. The baseline ONERA M6 configuration produced an L/D of 12.86, while the optimized configurations produced lower efficiency values, with o1 achieving an L/D of 8.79 and o3 achieving an L/D of 8.58. These results indicated that the model suggested geometric changes increased lift but increased drag by a larger margin, resulting in a reduction in aerodynamic efficiency.

Evidence for the reduction in L/D was the strengthened shock induced pressure recovery and the separation behavior in the optimized cases. In both o1 and o3, the static pressure contours exhibited a large pressure jump across the shock, with the pressure rising from the low pressure region on the upper surface toward approximately 100,000 Pa after the shock for o1. Additionally, the Mach contours demonstrated that the flow accelerated locally to supersonic values on the upper surface, reaching approximately Mach 1.4 for o1 and Mach 1.45 for o3 at the shock. The density contours showed compression across the shock, with density decreasing to approximately 0.8 kg/m^3 for o1 and 0.75 kg/m^3 for o3 ahead of the shock and increasing to approximately 1.1 kg/m^3 after the shock. The optimized airfoil and twist configurations produced increased wave drag and promoted a larger separated region downstream of the shock, which increased total drag and reduced L/D.

Unsteady behavior consistent with shock buffeting was observed in the optimized cases. The o1 case exhibited oscillatory aerodynamic coefficients, with C_L fluctuating between 0.51 and 0.53 and C_D fluctuating between 0.06 and 0.059. The o3 case exhibited similar behavior, with C_L varying from 0.56 to 0.59 and C_D ranging between 0.068 and 0.066. Although o3 produced higher lift than o1, it also produced a larger drag value. The presence of these oscillations further supported the conclusion that the flow field at this AoA and Mach number was sensitive to shock boundary layer interaction, limiting steady aerodynamic performance and reducing efficiency.

Overall, the results demonstrated that the optimized configurations did not improve the baseline ONERA M6 wing for the single operating point evaluated. The recommended airfoil change and twist distributions could alter shock structure in ways that may be beneficial at other angles of attack or Mach numbers but were not beneficial for Mach 0.84 and AoA 3.06°. It would have been better to analyze aerodynamic behavior on a range of flow conditions, including multiple angles of attack and potentially multiple Mach numbers, to determine whether the optimized configurations offered improvements under different operating points. Future work should therefore include a multi condition evaluation matrix that accounted for both aerodynamic efficiency and robustness to unsteady shock behavior.

References

[1] Li, Y., Zhao, H., Jiang, H., Pan, Y., Liu, Z., Wu, Z., Shu, P., Tian, J., Yang, T., Xu, S., Lyu, Y., Blenk, P., Pence, J., Rupram, J., Banu, E., Liu, N., Wang, L., Song, W., Zhai, X., Song, K., Zhu, D., Li, B., Wang, X., and Liu, T., "Large Language Models for Manufacturing," , 2024. URL `https://arxiv.org/abs/2410.21418`.

[2] Makatura, L., Foshey, M., Wang, B., Hähnlein, F., Ma, P., Deng, B., Tjandrasuwita, M., Spielberg, A., Owens, C. E., Chen, P. Y., Zhao, A., Zhu, A., Norton, W. J., Gu, E., Jacob, J., Li, Y., Schulz, A., and Matusik, W., “Large Language Models for Design and Manufacturing,” *An MIT Exploration of Generative AI*, 2024. Https://mit-genai.pubpub.org/pub/nmypmnhs.

[3] Wang, W., and Ma, J., “A review: Applications of machine learning and deep learning in aerospace engineering and aero-engine engineering,” *Proceedings of the 6th International Conference on Mechanical Engineering and Advanced Manufacturing*, Vol. 6, 2024, pp. 54–70. https://doi.org/10.54254/2977-3903/6/2024060, URL https://doi.org/10.54254/2977-3903/6/2024060.

[4] Zhang, Z., Ao, Y., Li, S., and Gu, G. X., “An adaptive machine learning-based optimization method in the aerodynamic analysis of a finite wing under various cruise conditions,” *Theoretical and Applied Mechanics Letters*, Vol. 14, No. 1, 2024, p. 100489. https://doi.org/10.1016/j.taml.2023.100489, URL https://www.sciencedirect.com/science/article/pii/S2095034923000600.

[5] Wang, L., Zhang, H., Wang, C., Tao, J., Lan, X., Sun, G., and Feng, J., “A Review of Intelligent Airfoil Aerodynamic Optimization Methods Based on Data-Driven Advanced Models,” *Mathematics*, Vol. 12, No. 10, 2024. https://doi.org/10.3390/math12101417, URL https://www.mdpi.com/2227-7390/12/10/1417.

[6] Schmitt, V., and Charpin, F., “Pressure Distributions on the ONERA-M6-Wing at Transonic Mach Numbers,” *Experimental Data Base for Computer Program Assessment. Report of the Fluid Dynamics Panel Working Group 04*, Advisory Group for Aerospace Research and Development (AGARD), NATO, 1979.

[7] Rumsey, C., “Turbulence Model Numerical Analysis,” , 2021. URL https://turbmodels.larc.nasa.gov/onerawingnumerics_val.html, accessed on 10 24, 2024.

[8] Diskin, B., Thomas, J., and Rumsey, C. L., “Grid Convergence for Turbulent Flows,” *53rd AIAA Aerospace Sciences Meeting*, 2015. https://doi.org/10.2514/6.2015-1745, URL https://arc.aiaa.org/doi/abs/10.2514/6.2015-1745.

[9] Thomas, B. Z., and Agarwal, R. K., *Application of Wray Agarwal Turbulence Model for Predicting Transonic Flow over ONERA-M6 Wing*, ???? https://doi.org/10.2514/6.2022-0463, URL https://arc.aiaa.org/doi/abs/10.2514/6.2022-0463.

[10] Mazumder, M. H. M., “Comparative study of turbulence models in CFD for transonic flow over the ONERA M6 wing,” *Discover Mechanical Engineering*, Vol. 3, 2024. https://doi.org/10.1007/s44245-024-00080-5, URL https://link.springer.com/article/10.1007/s44245-024-00080-5.

[11] Balan, A., Park, M. A., Anderson, W. K., Kamenetskiy, D. S., Krakos, J. A., Michal, T., and Alauzet, F., “Verification of Anisotropic Mesh Adaptation for RANS Simulations over ONERA M6 Wing,” *AIAA Journal*, Vol. 58, No. 4, 2020, pp. 1543–1563. https://doi.org/10.2514/1.J059158, URL https://ntrs.nasa.gov/citations/20200003084.

[12] Nambu, T., Hashimoto, A., Aoyama, T., and Sato, T., “Numerical Analysis of the ONERA-M6 Wing with Wind Tunnel Wall Interference,” *Transactions of the Japan Society for Aeronautical and Space Sciences*, Vol. 58, No. 1, 2015, pp. 7–14. https://doi.org/10.2322/tjsass.58.7, URL https://www.jstage.jst.go.jp/article/tjsass/58/1/58_T-14-19/_pdf.

[13] Ahrabi, B. R., Brazell, M. J., and Mavriplis, D. J., “An Investigation of Continuous and Discontinuous Finite-Element Discretizations on Benchmark 3D Turbulent Flows,” *57th AIAA Aerospace Sciences Meeting*, 2018. https://doi.org/10.2514/6.2018-1569, URL https://scientific-sims.com/cfdlab/Dimitri_Mavriplis/HOME/assets/papers/aiaa.2018.1569.pdf.

[14] Ilie, M., and Havenar, J., “Aeroelasticity of supersonic ONERA M6 wing; parametric studies using a fully-coupled computational approach,” *AIAA Aviation and Aeronautics Forum and Exposition, AIAA AVIATION Forum 2023*, American Institute of Aeronautics and Astronautics Inc, AIAA, 2023. https://doi.org/10.2514/6.2023-4089, publisher Copyright: © 2023, American Institute of Aeronautics and Astronautics Inc, AIAA. All rights reserved.; AIAA Aviation and Aeronautics Forum and Exposition, AIAA AVIATION Forum 2023 ; Conference date: 12-06-2023 Through 16-06-2023.